Materials Research Proceedings 54 (2025) 2037-2046 https://doi.org/10.21741/9781644903599-219

Friction stir welding (FSW) of 1200-O aluminum alloy: Temperature distribution modeling and metallurgical characterization

Geraldo T. Costa[1,a], Valdemar R. Duarte[2], Tarcísio G. Brito[1], Francisco W. C. Farias[2], Rafael Nunes[3], Gustavo H. S. F. L. de Carvalho[4], Gianni Campatelli[4], Bruno S. Cota[1]

[1]UNIFEI - Universidade Federal de Itajubá, Instituto de Engenharias Integradas, Itabira, MG, Brasil

[2]UNIDEMI, Department of Mechanical and Industrial Engineering, NOVA School of Science and Technology, Universidade NOVA de Lisboa, 2829-516, Caparica, Portugal

[3]IBS, Institut Belge de la Soudure, Gent, Belgium

[4]UNIFI, Università Degli Studi Di Firenze, Dipartimento di Ingegneria Industriale (DIEF), Florence, Italy

[a]d2020031741@unifei.edu.br

Keywords: Friction Stir Welding, Computer Simulation, AA1200 Aluminum Alloy

Abstract. In recent years, the Friction Stir Welding (FSW) process has emerged as an efficient technique for joining metals. This work evaluates a thermomechanical model developed to analyze FSW parameters on 3 mm thick 1200-O aluminum sheets, using tools with conical and cylindrical pins. The research was divided into two stages: virtual and experimental. The virtual model simulated the welding parameters and predicted the thermal and mechanical behavior of the joints. In the experimental stage, welding was carried out on an adapted conventional milling machine, with real-time thermal monitoring. Tensile, bending, microhardness and microstructural analysis tests revealed weld seams with good visual quality and tensile efficiencies of 64.82% for the conical pin and 66.06% for the cylindrical pin.

Introduction

Friction stir welding (FSW) with a non-consumable pin is a solid-state welding method. The process was developed by Wayne Thomas and a group of researchers in the early 1990s in Cambridge, UK, and its remarkable growth can be explained by the possibility of successfully joining materials that were previously considered un-weldable or difficult to weld [1].

The FSW process is able to minimize problems commonly found in other conventional welding processes. Some of the benefits of the FSW method include fine microstructures, low residual distortion and absence of cracks [2]. Its application is wide-ranging, covering various types of joints and materials, including dissimilar alloys.

Optimizing the FSW welding process still presents challenges, due to the ability of welding parameters and tool characteristics to significantly influence the results. This study examines FSW applied to 1200-O aluminum alloy, with butt joints welded using tools of different geometries. The aim is to evaluate the influence of thermal inputs on the microstructure and mechanical performance of the joints.

Virtual Model Development

The process of building the virtual non-linear thermomechanical model for simulating FSW welding was carried out using the Altair HyperWorks computer package (version 2019.1). The model considered butt welding, with the plate clamped at the ends, as well as taking into account the influence of convection, conduction and plastic deformations of the joint.

Due to technical limitations in the software used, the simulation was unable to accurately reproduce the 10° taper of the tapered pin. Even so, the analysis and conclusions were made considering the theoretical configuration of the tool, ensuring that the results interpreted the expected characteristics of the taper.

Since sliding is the predominant condition, the coefficient of friction should reach values between 0.27 and 0.35 [3]. In this study, it was decided to adopt the average value of 0.30. Since there is no measured experimental data available, only theoretical values were considered for the heat losses on the top and bottom surface of the plate, as well as on the tool, by convection. Thus, convective coefficients were used, which remained constant, following the methodology used by Pires, Cota, Bracarense and Campolina [4]. The parameters considered in the FSW process are shown in Table 1.

Table 1 – Process parameters

Property	Unit	Value
Sheet widht	[mm]	250
Sheet thickness	[mm]	3
Sheet length	[mm]	400
Initial sheet temperature	[ºC]	27
Surface convective coefficient	[W/m² ºC]	20
Tool convective coefficient	[W/m² ºC]	10
Bench convective coefficient	[W/m² ºC]	300
Coefficient of friction	[-]	0,3
Specific mass	[kg/cm³]	2700
Specific Heat at Constant Pressure	[J/kg-K]	900
Thermal Conductivity	[W/m-k]	230
Coefficient of Thermal Expansion	[µm/m-K]	23
Liquidus Temperature	[ºC]	660
Solidus Temperature	[ºC]	650
Young's Modulus of Elasticity	[GPa]	69
Poisson's ratio	[-]	0,33
Rotational speed	[RPM]	1180
Translation speed	[mm/min]	95
Penetration	[mm]	2,9
Direction of rotation	[Clockwise]	[-]
Dwell time	[s]	14
Immersion speed	[mm/min]	10

Alloy 1200-O, belonging to the 1XXX series, is composed (in % by weight) of 99% aluminum (min.). The complete chemical composition of aluminum alloy 1200 is shown in Table 2.

Table 2 – Chemical composition of aluminum alloy 1200 (%)

Al	Si	Fe	Cu	Mn	Mg	Cr	Zn	Ti	Outros (Cada)	Outros (Total)
99	1,00 (Si + Fe)	-	0,05	0,05	-	-	0,10	0,05	0,05	0,15

Definition of Boundary Conditions and Mesh Generation

As for the thermal boundary conditions, which refer to the heat generated by both friction and plastic deformation in the process, Patel and Patil [5] comment that these heat losses occur by convection and radiation on the upper and lateral surfaces of the part, while on the lower surface heat is conducted towards the support plate.

With regard to mesh generation, the HyperMesh finite element processor, integrated into HyperWeld, uses the Automesh module to automatically generate high-quality meshes based on the geometries present. This module creates meshes on specified surfaces, taking into account the edge length of the elements. For this work, the automatically generated mesh was considered adequate.

Development of the Experimental Model

The equipment used in this study is a universal milling machine, model FUH-5 (X6036), manufactured by EUROSTEC, and located in the Machining Laboratory of UNIFEI - Campus Theodomiro Carneiro Santiago.

The specific mechanical properties of the 1200-O aluminum alloy are detailed in Table 3, where σ_y represents the yield strength, $\sigma_{mín}$ - $\sigma_{máx}$ indicates the tensile strength range and ε represents the minimum elongation.

Table 3 – Mechanical properties of aluminum alloy 1200

Alloy	σ_y [MPa]	$\sigma_{mín} - \sigma_{máx}$ [MPa]	ε [%]	Brinell Hardness [HB]
1200-0	25	75 - 105	22	23

About the tools used, the difference in geometry lies in the pin configuration, with one tool having a conical pin and the other a cylindrical pin. According to Khan, Siddiquee and Khan [6], solid-state welding can be carried out at high temperatures, but without melting the joined materials. H13 tool steel is highly recommended for this application. (Fig. 1) illustrates the geometry and construction dimensions of the tools used.

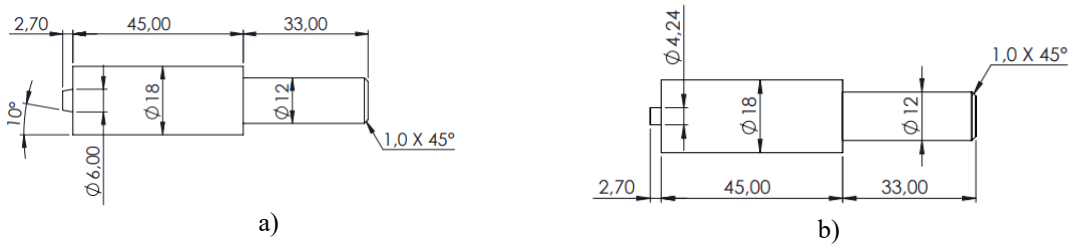

Figure 1 – Tools used in the FSW process, a) with conical pin geometry and b) with cylindrical pin geometry.

The temperature on the aluminum plate was monitored by a FLIR E40 thermographic camera, provided by the Power Generation Laboratory at UNIFEI - Theodomiro Carneiro Santiago Campus. The equipment has a thermal sensitivity (Noise Equivalent Temperature Difference - NETD) of < 0.07ºC at 30ºC, an infrared detector with 19,200 (160 × 120) pixels and an operating temperature range of -20 °C to 650 °C (-4 °F to 1202 °F). For the tests, it was configured for materials with an emissivity of 0.97, following the manufacturer's table.

The final assembly of the thermal imaging camera in relation to the welding bench is shown in (Fig. 2).

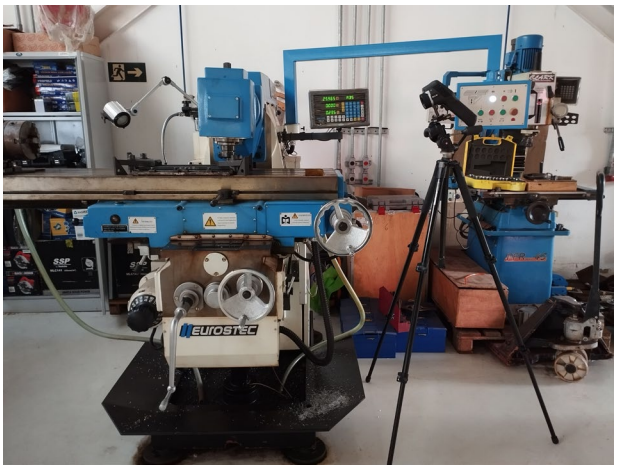

Figure 2 – Final assembly of the thermographic camera for data acquisition: positioned along the direction of the welding tool

To improve the camera's detection of the infrared spectrum, the base metal to be welded was painted black to increase its emissivity, bringing it close to 1, so that it behaved like a black body.

Virtual Stage Results

Thermal analysis of the friction stir welding (FSW) process with a tapered pin tool revealed a maximum temperature of 598ºC (Fig. 3a), representing around 90.6% of the melting temperature of the alloy used. The Mixed Zone (MZ) (nugget) showed characteristic distortions attributed to the flow of material during welding, influenced by the geometry of the tool, rotation, translation and movement of the material [4]. Differences in cooling times between the feed side (LA) and the retreat side (LR) resulted in higher temperatures and tensile stresses in the LA [7]. Using the Node Path feature (Fig. 3b) in HyperView, the thermal profile of the weld was plotted, showing an inflection in the temperature curve and higher temperatures on the forward side.

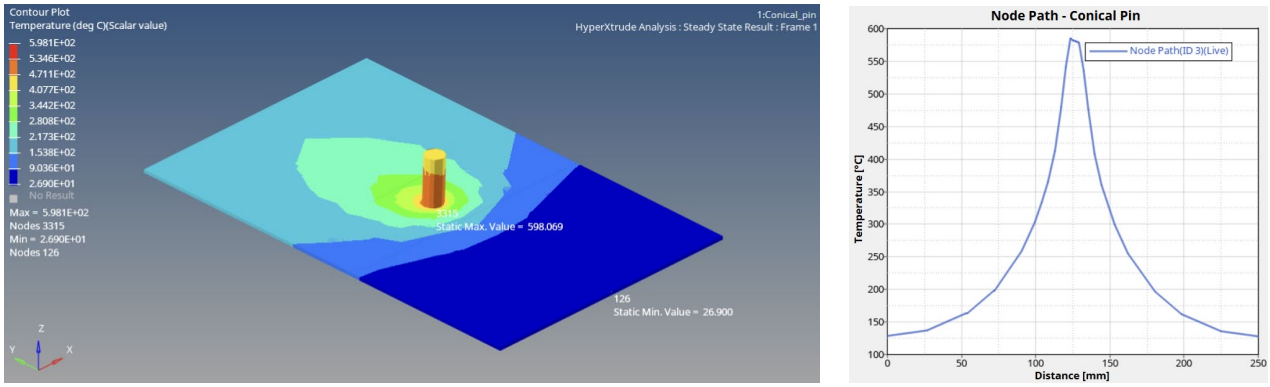

a) b)

Figure 3 – Virtual numerical temperature distribution for the 1200-O alloy during the FSW process using the tapered pin tool

The maximum temperature obtained using the tool with a cylindrical pin geometry was 506ºC (Fig. 4a). Since the melting temperature of the 1200-O aluminum alloy is 660ºC, approximately 70.7% of this value was reached. The analysis using the Node Path feature is shown in (Fig. 4b). Again, the thermal analysis allowed us to see an inflection in the temperature curve, and higher temperatures on the feed side.

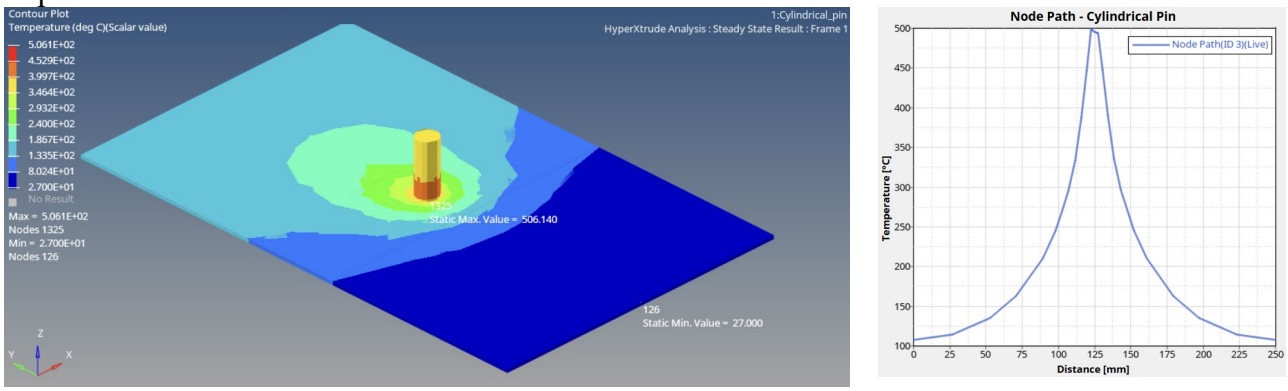

a) b)

Figure 4 – Virtual numerical temperature distribution for the 1200-O alloy during the FSW process using the cylindrical pin tool

Temperature difference

According to Bokov et al [8], the main factor in heat generation in FSW is the contact area between the tool and the workpiece. In the virtual tests, the temperature differences observed were attributed to the different geometries of the tool pins.

To analyze this relationship, the areas of the pins of each of the tools were calculated, considering the exact geometries of the tools used in the simulation. The areas calculated for each of the regions and the heat generated in the respective areas are shown in Table 4.

The temperatures were calculated based on the average of 10 different points in each area of interest, using the Node Path feature available in the software.

Table 4 – Tool areas and heat generated, a) tool with conical pin geometry and b) tool with cylindrical pin geometry

Region	Area [mm²]		Temperature generated [ºC]	
	a)	b)	a)	b)
Shoulder (bottom)	226,19	240,35	512	442
Pin tip	28,27	14,12	593	504
Side of pin	50,89	35,96	582	497
Total area	305,32	290,43	[-]	[-]

The geometric analysis shows that the total area of pin a) is slightly larger than the total area of pin b). The tool with the cylindrical pin has a temperature below the maximum temperature allowed in the welding process in question. When compared, its percentage difference (14.80%) reflects 138°C below the maximum temperature, while the tapered pin tool reflects 4°C (0.69%) above the maximum temperature allowed in the process. This directly influences the efficiency of the process, since a larger area generates more heat and improves the plasticity of the material in regions where welding is critical, while a smaller area tends to reduce the thermal input, which may not be sufficient in certain cases to guarantee adequate fusion of the materials and the integrity of the weld.

Experimental Virtual Correlation

Fig. 5 shows the temperature profile during the welding of the sheets with the tapered pin tool, at different stages of the process: a) beginning of the weld bead, b) and c) center, and d) end of the bead.

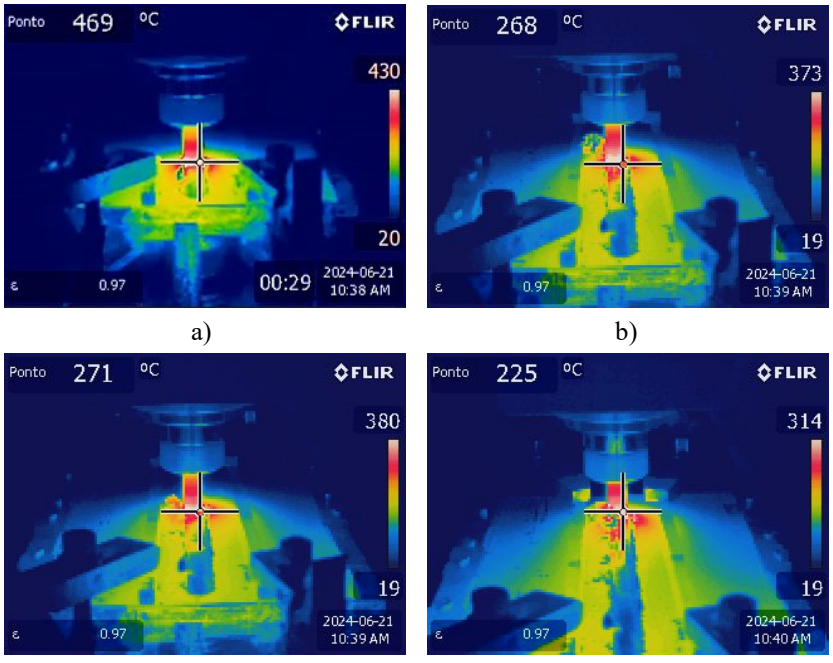

Figure 5 – Thermographic images of the plate welded by the tapered pin at different times

The highest temperature captured by the thermal camera, when using the tapered stud tool, was 469 ºC, as indicated on the left in (Fig. 5 a)). According to the simulation, the maximum temperature expected for the process with the tapered pin was 598 ºC.

The experimental surface temperature results showed a limited approximation to the virtual model, with a deviation of 21.57% between the highest simulated temperature and the experimental measurement, exceeding the 10% margin generally accepted in friction stir welding simulations [9]. This deviation can be attributed to the high non-linearity of the process and the data collection methodology, carried out using photographs rather than continuous video, possibly not capturing the maximum temperature of the process.

(Fig. 6) shows the temperature profile during the welding of the sheets with the cylindrical pin tool, again at different stages of the process: a) beginning, b) and c) center, and d) end of the bead.

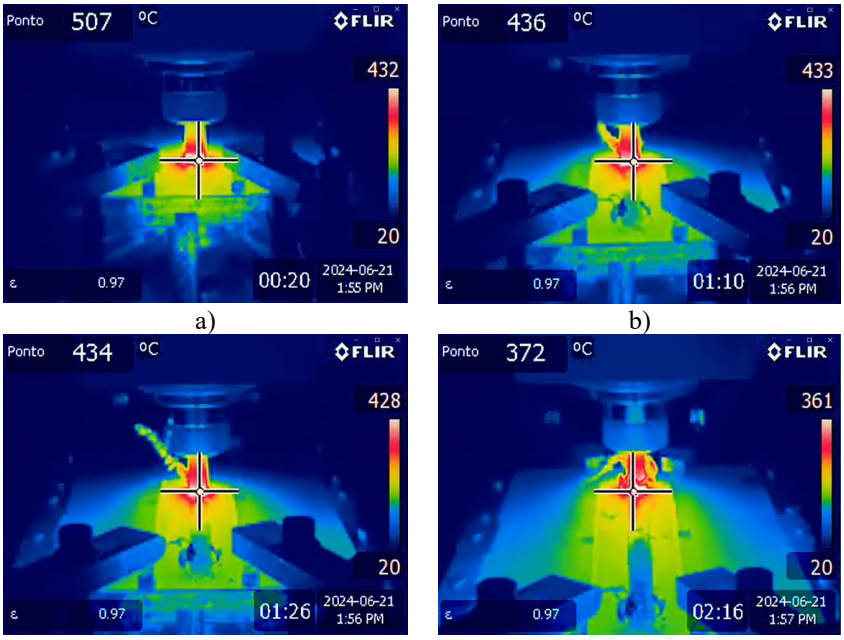

Figure 6 – Thermographic images of the plate welded by the cylindrical pin at different times

The highest temperature recorded by the thermal camera, when using the cylindrical pin tool, was 507 ºC, as shown on the left in (Fig. 6 a)). According to the simulation, the expected maximum temperature was 506 ºC.

The virtual model for the cylindrical pin tool showed a high correspondence with the experimental results. The maximum temperature recorded experimentally was practically the same as that predicted by the simulation, with an error of just 0.19%.

Results of the Experimental Stage

The results of the mechanical properties of the welded specimens, when compared to the properties of the base material, show relatively satisfactory efficiencies. The values obtained are shown in Table 5.

Table 5 – Efficiencies of welded joints

Aluminum alloy	Efficiency [%]		
	σ_y	$\sigma_{máx}$	ε
1200 – O	62,14	64,82	34,50
1200 – O	60,80	66,06	43,23

Visual analysis of the bending tests revealed satisfactory results in both cases. No cracks, fissures or ruptures were observed.

Materials Research Proceedings 54 (2025) 2037-2046 https://doi.org/10.21741/9781644903599-219

Metallographic analysis was carried out to examine the microstructure of the FSW welded joints. (Fig. 7) shows a visual analysis of the welded region immediately after chemical etching. In both samples, the appearance of a defect known as a remnant joint line was observed.

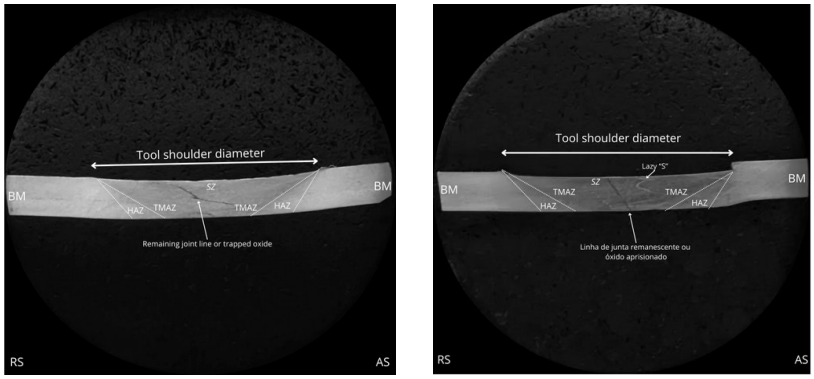

a) b)

Figure 7 – Visual analysis of samples with conical pin a) and cylindrical pin b)

According to Le Jolu et al [10], FSW welds in aluminum often present discontinuous and wavy surfaces in the nugget, known as kissing bond, lazy S or entrapped oxide defect, resulting from an almost continuous oxide layer in the welded zone. Mishra and Mahoney [11] attribute this defect to factors such as inadequate surface cleaning, incorrect tool alignment, excessive welding speeds or inadequate shoulder diameters, which lead to insufficient deformation at the interface.

Optimized parameters, such as tool rotation and inclination, can mitigate the formation of this defect [12]. In the present study, the microstructure of the cross section of the weld with the cylindrical pin (Fig. 7 b)) revealed the presence of the lazy S defect, characterized by a black wavy line associated with the extrusion and deformation of oxides during FSW.

The macro-structures of the welded joints were analyzed using a Scanning Electron Microscope (SEM) (Figs. 8 and 9), at magnifications of 1000x and 5000x in different regions (edge and center), allowing the characteristics of the defects and welded zones to be identified.

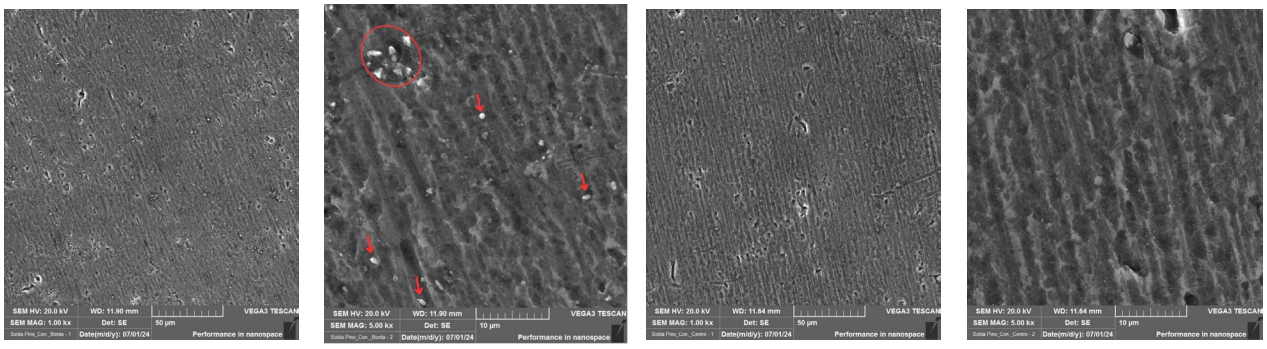

a) b) c) d)

Figure 8 – made with cylindrical pin, a) edge magnified at 1000x, b) edge magnified at 5000x, c) center magnified at 1000x, d) center magnified at 5000x

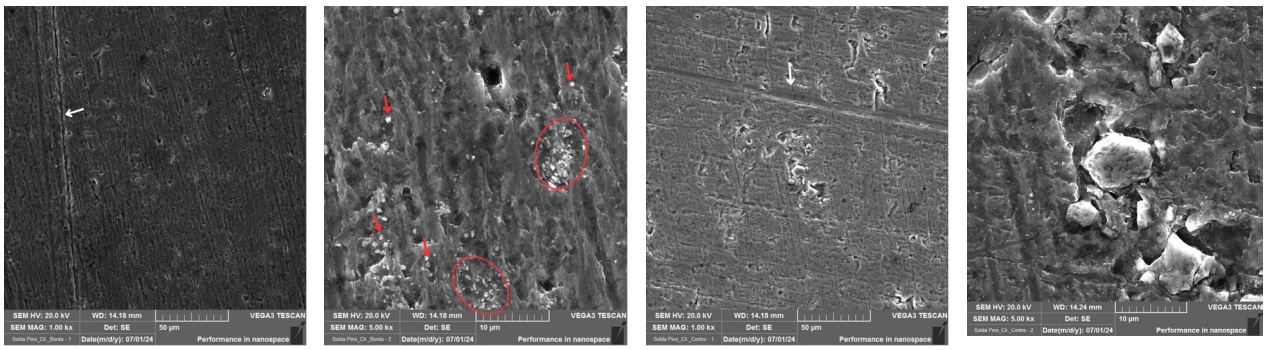

a) b) c) d)

Figure 9 – Sample made with cylindrical pin, a) edge magnified by 1000x, b) edge magnified by 5000x, c) center magnified by 1000x, d) center magnified by 5000x

We observed the growth of precipitates and agglomerates in the region of the base material (Fig. 8 b) and 9 b)). (Fig. 9 a) and c)) indicate defects caused by the sample preparation process, such as channels possibly left by sandpaper grains or scratches after grinding and polishing.

In the central regions of the samples (Fig. 8 c), d) and 9 c), d)), high temperatures solubilized precipitates, resulting in a loss of hardness. However, dynamic recrystallization, due to the high degree of plastic deformation and thermal input, has the ability to refine the grains, balancing the loss of hardness with a more homogeneous and resistant microstructure [13-14].

The graph (Fig. 10) shows microhardness values, with the zero point marking the center line of the weld and the positive axis representing the feed side. The average hardness of the base metal was 45.42 HV, used as a reference for the welds.

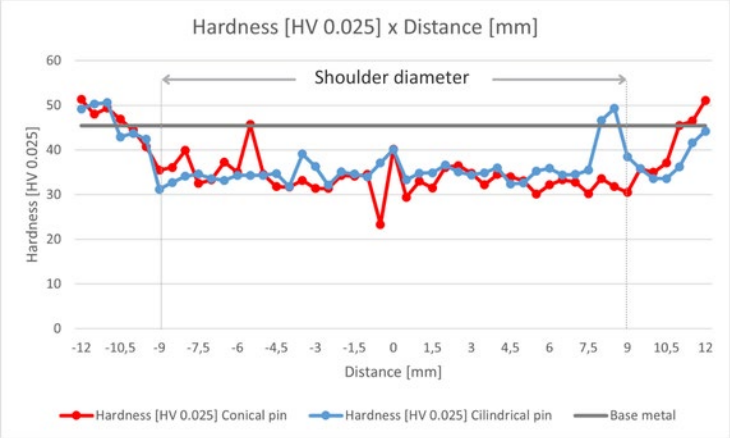

Figura 10 – Microhardness profile of tools

For the tool with the tapered pin, the average hardness was 36.27 HV, representing a reduction of 20.16% (9.15 HV) compared to the base metal, with an average standard deviation of 6.23 HV. In the central region, corresponding to the diameter of the shoulder, the hardness was 33.66 HV, a reduction of 25.90%. For the tool with the cylindrical pin, the average hardness was 37.07 HV, a reduction of 18.39% (8.35 HV), with an average standard deviation of 5.13 HV. In the central region, the hardness was 34.96 HV, corresponding to a reduction of 23.03%.

For both tools, the original hardness of the base metal was recovered around 12 mm from the center line of the weld, indicating a zone of hardness loss concentrated around 24 mm from the center line.

Conclusions

Simulations carried out in Altair HyperWorks analyzed the thermal effects in FSW welding of aluminium sheets with different tools, identifying thermal variations of up to 15.38% in the

distribution and simulated deviations of 21.57% for the tapered pin and 0.19% for the cylindrical pin. Tensile tests indicated average efficiencies of 64.82% (conical pin) and 66.06% (cylindrical pin), while bending tests confirmed high ductility, with no cracks. The microhardness showed a drop of up to 26% in the mixing zone, due to plastic deformation and thermal input, with metallurgical transformations observed in this region. Metallographic images showed changes in the base material, but adjustments in sample preparation are needed for more accurate future analysis.

References

[1] J. P. Pires, B. S. Cota, A. Q. Bracarense, and B. A. Campolina, "Predição da Distribuição de Temperatura em Juntas da Liga de Alumínio 5052 H34 Soldadas pelo Processo Friction Stir Welding," *Soldagem & Inspeção*, vol. 23, no. 2, pp. 247–263, Jun. 2018. https://doi.org/10.1590/0104-9224/si2302.11.

[2] S. Thamizhmanii, M. A. Sukor, and Sulaiman, "Solid State Friction Stir Welding (FSW) on Similar and Dissimilar Metals," Proceedings of the World Congress on Engineering, vol. 3, pp. 1743–1748, Jul. 2013.

[3] H. Schmidt, J. Hattel, and J. Wert, "An analytical model for the heat generation in friction stir welding," *Modelling and Simulation in Materials Science and Engineering*, vol. 12, no. 1, pp. 143–157, Jan. 2004. https://doi.org/10.1088/0965-0393/12/1/013.

[4] J. P. Pires, B. S. Cota, A. Q. Bracarense, and B. A. Campolina, "Predição da Distribuição de Temperatura em Juntas da Liga de Alumínio 5052 H34 Soldadas pelo Processo Friction Stir Welding," *Soldagem & Inspeção*, vol. 23, no. 2, pp. 247–263, Jun. 2018. https://doi.org/10.1590/0104-9224/si2302.11.

[5] J. B. Patel and H. S. Patil, "Simulation of Peak Temperature & Flow Stress during FSW of Aluminium Alloy AA6061 for Various Tool Pin Profiles," *International Journal of Materials Science and Engineering*, 2014. https://doi.org/10.12720/ijmse.2.1.67-71.

[6] N. Z. Khan, A. N. Siddiquee, and Z. A. Khan, *Friction Stir Welding*. CRC Press, 2017. doi: 10.1201/9781315116815.

[7] D. M. Souza, H. C. Pinto, J. F. Santos, and R. S. Coelho, "Estudo das propriedades mecânicas, microestruturais e tensões residuais da liga de alumínio AA 5083-H111 soldadas por Friction Stir Welding - FSW," Rio de Janeiro, 2015.

[8] D. O. Bokov *et al.*, "Effect of Pin Shape on Thermal History of Aluminum-Steel Friction Stir Welded Joint: Computational Fluid Dynamic Modeling and Validation," *Materials*, vol. 14, no. 24, p. 7883, Dec. 2021. https://doi.org/10.3390/ma14247883.

[9] N. Sibalic and M. Vukcevic, "Numerical Simulation for FSW Process at Welding Aluminium Alloy AA6082-T6," *Metals*, vol. 9, no. 7, p. 747, Jul. 2019. https://doi.org/10.3390/met9070747.

[10] T. le Jolu *et al.*, "Microstructural Characterization of Internal Welding Defects and Their Effect on the Tensile Behavior of FSW Joints of AA2198 Al-Cu-Li Alloy," *Metallurgical and Materials Transactions A*, vol. 45, no. 12, pp. 5531–5544, Nov. 2014. https://doi.org/10.1007/s11661-014-2537-1.

[11] R. S. Mishra and M. W. Mahoney, *Friction stir welding and processing*. ASM International, 2007.

[12] N. Dialami, M. Cervera, M. Chiumenti, and A. Segatori, "Prediction of joint line remnant defect in Friction Stir Welding," *International Journal of Mechanical Sciences*, vol. 151, pp. 61–

69, 2019, Accessed: Aug. 09, 2024. [Online]. Available: https://upcommons.upc.edu/bitstream/handle/2117/132737/23536484.pdf;jsessionid=FF8BA78DCCEAFE0638EE12E9F90E440E?sequence=1

[13] D. T. Almeida, “Análise microestrutural e avaliação mecânica de juntas soldadas por fricção e mistura mecânica (FSW) da liga de alumínio 5182-O,” Porto Alegre, 2015.

[14] A. Davenport *et al.*, “Corrosion of friction stir welds in high strength aluminium alloys,” 2003.